Confined Synthesis of $BiVO_4$ Nanodots and ZnO Clusters Co-decorated 3DOM TiO_2 for Formic Acid Production from Xylan-based Hemicellulose Photorefinery

Heng Zhao [a, b], Xinti Yu [a], Guichun Hu [a], Na Zhong [a], Zhi-Yi Hu [b, c], Steve Larter [d], Yu Li [b, c*], Md Golam Kibria[a*], Jinguang Hu [a*]

[a] Department of Chemical and Petroleum Engineering, University of Calgary, 2500 University Drive, NW, Calgary, Alberta T2N 1N4, Canada.

[b] State Key Laboratory of Advanced Technology for Materials Synthesis and Processing, Wuhan University of Technology, 122 Luoshi Road, 430070 Wuhan, Hubei, China.

[c] Nanostructure Research Centre, Wuhan University of Technology, 122 Luoshi Road, 430070 Wuhan, Hubei, China.

[d] Department of Geosciences, University of Calgary, 2500 University Drive, NW, Calgary, Alberta T2N 1N4, Canada.

[*]To whom correspondence should be addressed. Email: yu.li@whut.edu.cn, md.kibria@ucalgary.ca, jinguang.hu@ucalgary.ca

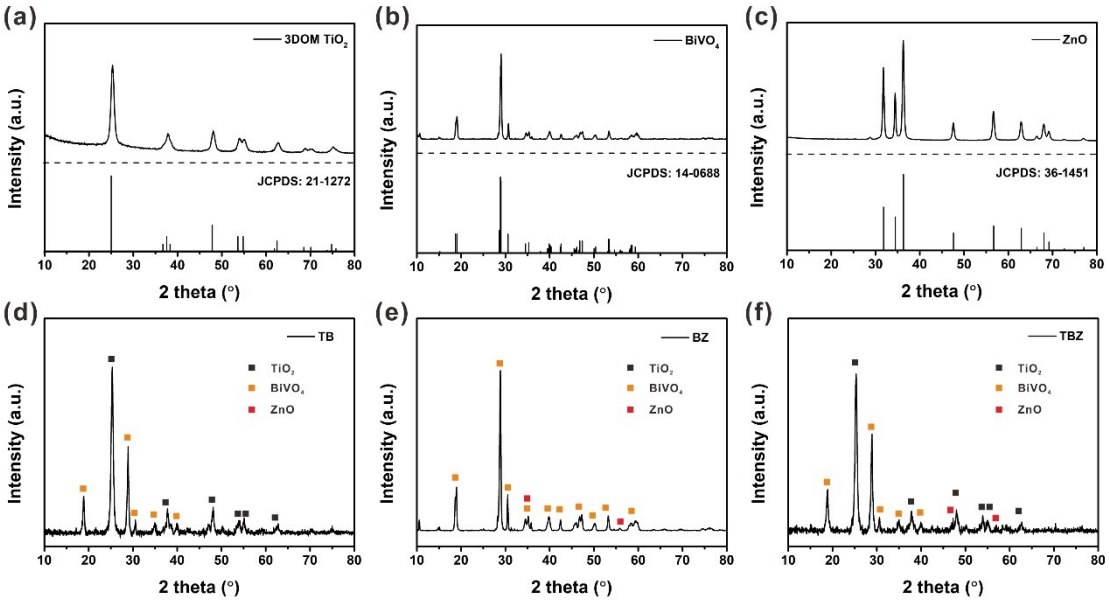

Fig. 1. XRD patterns of (a) 3DOM TiO_2, (b) $BiVO_4$, (c) ZnO, (d) TB, (e) BZ, (f) TBZ.

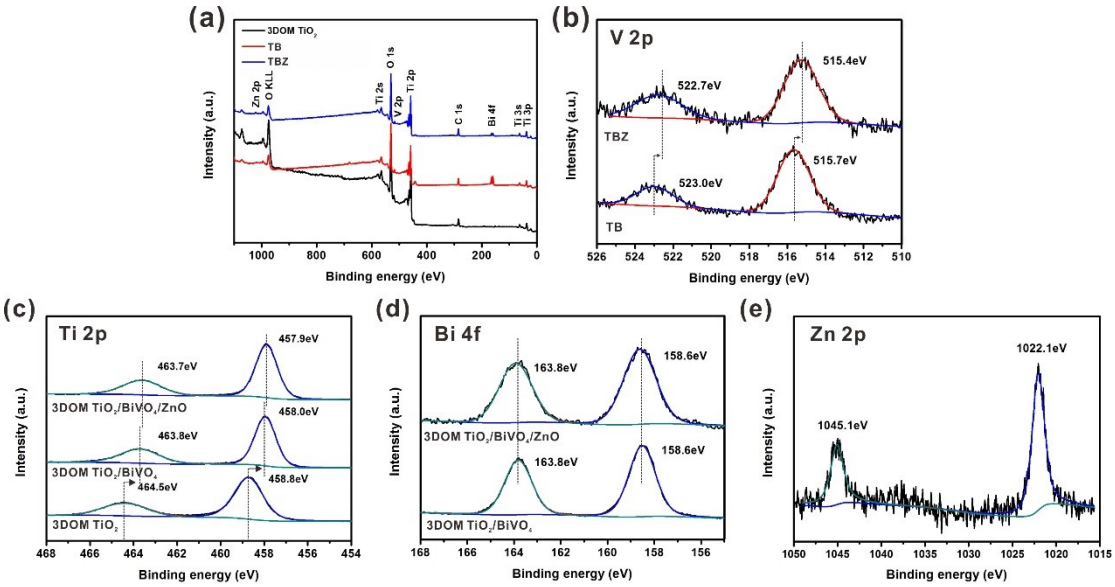

Fig. 2. (a) XPS survey spectra of 3DOM TiO_2, TB and TBZ, high-resolution XPS spectra of (b) V 2p, (c) Ti 2p, (d) Bi 4f and (e) Zn 2p.

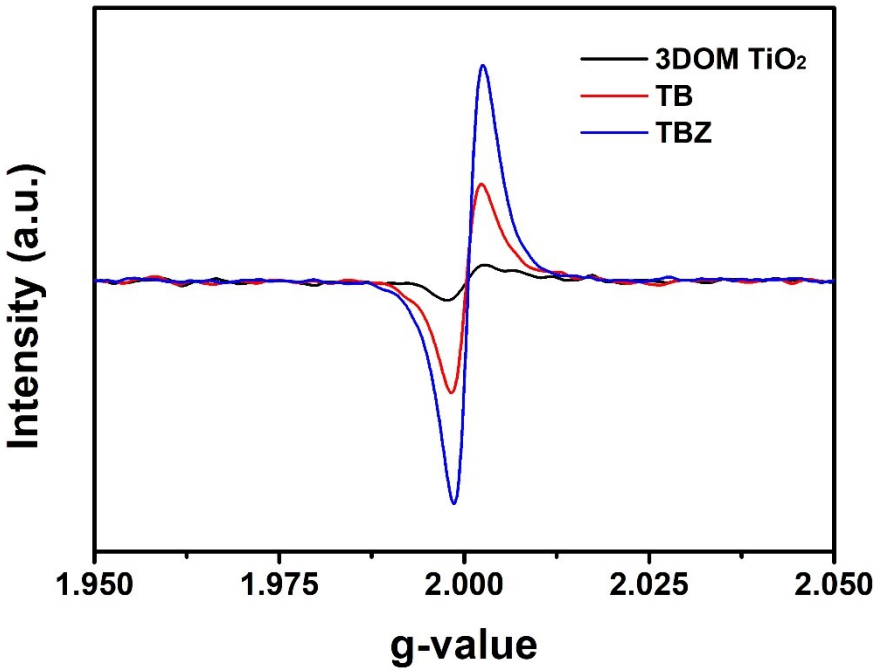

Fig. 3. ESR spectra of oxygen vacancies in different photocatalysts.

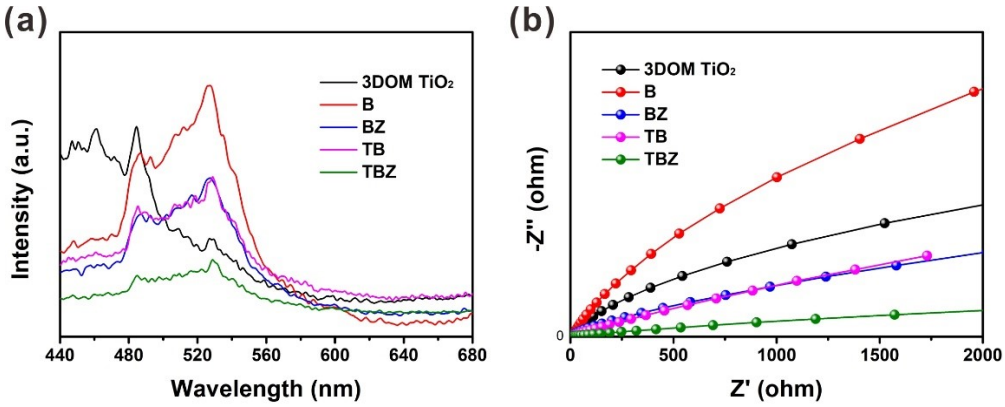

Fig. 4. (a) PL spectra with 420 nm excitation wavelength and (b) EIS Nyquist plots of all the photocatalysts.

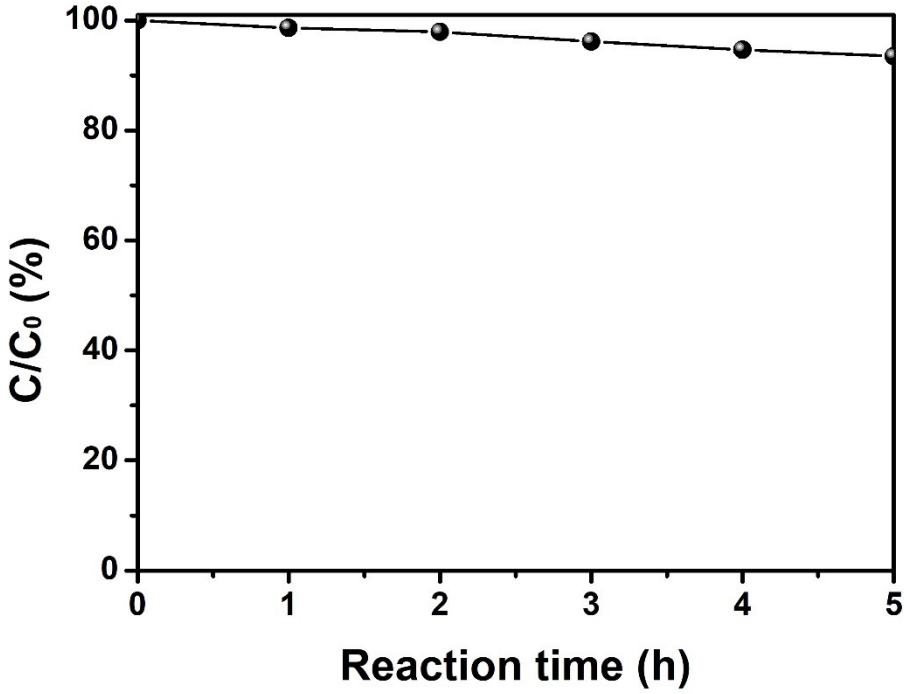

Fig. 5. Formic acid photodegradation over TBZ.

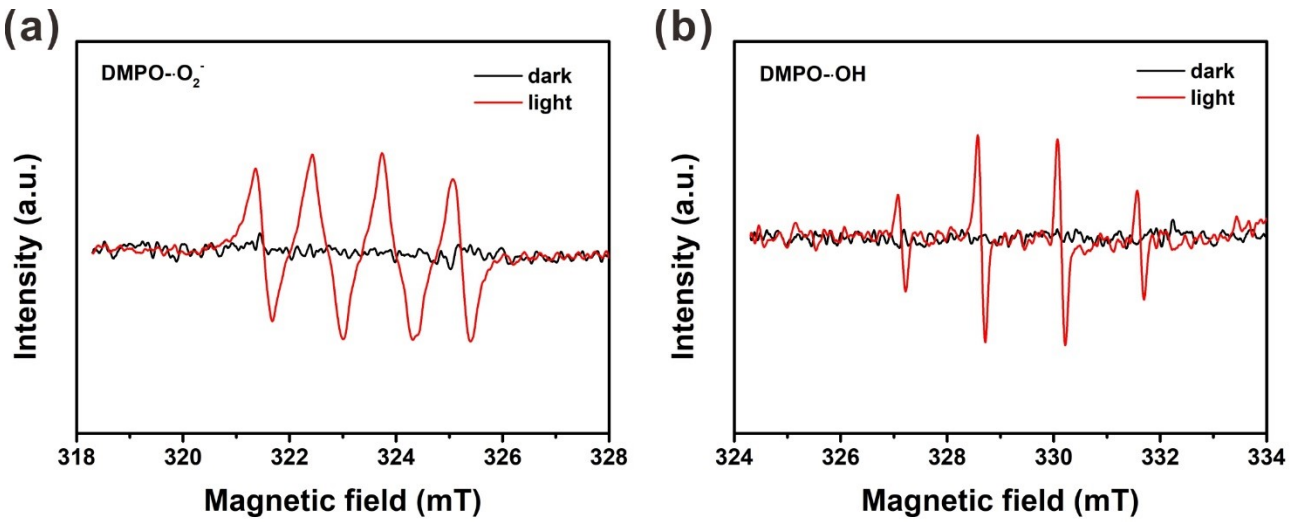

Fig. 6. ESR signal for the detection of (a) $\cdot O_2^-$ and (b) ·OH under dark and light condition over TBZ photocatalyst.

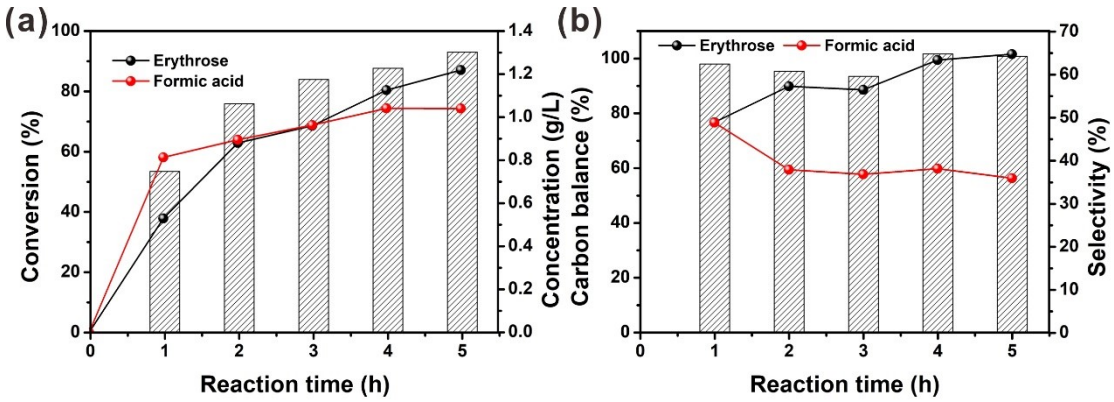

Fig. 7. (a) Arabinose conversion with product distributions, (b) calculated carbon balance and product selectivity over TBZ in O_2 atmosphere.